Journal of
Water & Climate Change

IWA PUBLISHING

Journal of Water and Climate Change Vol 14 No 4, 1112 doi: 10.2166/wcc.2023.248

Hydrological response to climate change in the Deme watershed, Omo-Gibe Basin, Ethiopia

Habtamu Daniel

College of Engineering, Hydraulic and Water Resources Engineering, Wolaita Sodo University, Wolaita Sodo, Ethiopia
E-mail: habtedanny12@gmail.com

HD, 0000-0002-6591-2364

ABSTRACT

Climate change is believed to have led to changes in global patterns. This study evaluated the hydrological responses to climate change in the Deme watershed using the Soil and Water Assessment Tool (SWAT) for two consecutive periods of 2031–2050 and 2051–2070. Climate variables were downscaled from RACMO22T, under RCP4.5 and RCP8.5 scenarios from CORDEX-Africa. Distribution mapping and variance scaling methods were used for bias correction of precipitation and temperatures, respectively, and for further analysis. The SWAT model was calibrated (and validated) for the 1989–2000 (2001–2010) period, and the hydrological model showed a reasonably good agreement. The result shows that the rainfall and streamflow show a decreasing signal in the wet season. The maximum projected change in annual temperature, PET, and ET was 2.15 °C, 10.89, and 9.24%, respectively, in the far future period under the RCP8.5 scenario. These incremental changes have an impact on declining annual rainfall and streamflow up to 27.6 and 26.2%, respectively, under the RCP8.5 scenario in 2031–2050. The subsequent results were the maximum decline of surface runoff by 15.10%, groundwater by 14.78%, and total water yield by 26.10% in 2031–2050 under the RCP8.5 scenario. Thus, the concerned body integrates its duties with climate change.

Key words: climate change, Deme watershed, hydrology, RCM, RCPs, SWAT

HIGHLIGHTS

- Distribution mapping and variance scaling methods were used for bias correction.
- Rainfall and streamflow show a decreasing signal in wet seasons compared to dry seasons in the watershed.
- Temperature and evapotranspiration are directly related, and inversely related to rainfall, streamflow, surface runoff, groundwater, and total water yield in the watershed.

1. INTRODUCTION

Nowadays, scientific evidence is demonstrating the mean temperature of the earth's surface is rising as a result of greenhouse gas emissions, and other natural and human activities (Shiferaw *et al.* 2018). Earth's temperature is determined by the balance between the inward solar radiation and the outward terrestrial radiation. The energy coming in the form of the sun can pass through the atmosphere and heats the surface of the earth. Then, the radiation emitted from the surface of the earth is partly absorbed by some gases in the atmosphere and some of it is re-emitted downwards (Legesse *et al.* 2015). This increase in surface air temperature has a high probability to affect the hydrologic cycle. The hydrological cycle is the driving factor for the physical and ecological processes on the earth's surface and has a huge impact on the survival of living organisms, particularly human beings (Rakhimova *et al.* 2020). Changes in the hydrological cycle led to the increasing occurrence of extreme events, related to each aspect of human activity; influencing agricultural activities, ecosystems, groundwater, water supply, energy production, land use, and the quantity and quality of regional water resources (Biniyam & Abdella 2017). Climate change affects the function and operation of existing water infrastructures including hydropower, structural, drainage, and irrigation systems as well as water management practices (Chaemiso *et al.* 2016). The atmosphere and ocean have warmed, the quantities of snow and ice have reduced, and the sea level has risen. Many aspects of climate alteration and its associated effects will continue for centuries, even though anthropogenic emissions of greenhouse gases are stopped

(IPCC 2014; Raneesh 2014). The warmer temperatures will upsurge the water-holding capacity of air resulting in higher moisture contents, thus creating forceful rainfall and snow events (Gunathilake *et al.* 2020). Therefore, understanding the hydrological process is essential for planning and managing water resources. Greenhouse gas enhancement is unequivocal at global scales resulting from increasing driving forces for future expansion of emissions of substances. Climate change and warming of temperature is a global issue, and its effect is not restricted to the unique region.

Watersheds are very sensitivity to climate change and uncertainty due to the hydrological impacts of climate change in the watershed areas. The comparison between monthly and annual streamflows between the baseline and future periods shows a high variation in the four watersheds despite their proximity in the upper catchments of the Nzoia river basin in western Kenya (Musau *et al.* 2015). The watersheds located at the same region can definitely show different degrees of hydrological responses to the same external climate changes. The differences in spatially distributed physical catchment properties play a main role in the sensitivity of catchments to varying climate conditions. Expected rise in precipitation and temperature resulted in upsurged total available streamflow, with a lower spring and summer streamflow, but a considerably higher winter streamflow. Also, significant changes in flow durations with lower chances of both high and low flows can be projected in boreal Sweden in the future (Teutschbein *et al.* 2015). It is vital to evaluate variations in low flow across the watershed and basin, because it is suffering from water shortage and salt water intrusion in the dry season. The variation of river discharge is likely to aggravate water stress. Particularly the reduction of low flow is a problematic. The results of the study in the Pearl River basin in the south of China, using five different climate models under the RCP4.5 and 8.5 scenarios, indicate a reduction in average low flows under all climate models. The decline varies across the basin and in between 6 and 48% under the RCP4.5 scenario. The river discharge in the dry season is expected to reduce throughout the basin. However, in the wet season, river discharge tends to increase in the middle and lower reaches and decrease in the upper reach of the Pearl River basin (Yan *et al.* 2015).

Developing countries, particularly sub-Saharan Africa, are likely to be especially vulnerable to climate change as recurrent floods and droughts continue to bring misery to millions in Africa, due to lack of institutional capacity and economic development (IPCC 2013; Wagesho *et al.* 2013). Therefore, linking watershed management with climate change adaptation and mitigation is mandatory in African countries (Joosten & Grey 2017).

Ethiopia is one of the most vulnerable countries to climate change and the least ready to improve resilience. The severe drought of 2015–2016 was worsened by the strongest El Nino, causing successive harvest failures and widespread livestock deaths in some regions. It has experienced even more major floods in different parts of the country (Disasa *et al.* 2019). Generally, the climate change impact in Ethiopia is signified by frequent and severe droughts, floods, increases in temperature, erratic and uneven rainfall, shifts in the onset and cessation of seasonal rainfalls, water stress, and scarcity. There have also been increased heat waves and windy days, increased health risks (malaria, diarrhea, and malnutrition), hailstorm and frost in some areas, increased landslides, and soil erosion problems in many parts of the country. Accordingly, crop failure is the most common problem in Ethiopia (Hagos 2019). Deforestation is the main cause of climate variability, and it is the major problem in Ethiopia (Tesfaye 2017).

Large parts of Ethiopia are arid and semi-arid regions that are highly vulnerable to climate change. Also, a large number of populations are poor with an agricultural-based economy, and the country faces extensive deforestation. Moreover, it has a low adaptive capacity to deal with the consequences of climate variability (World Bank 2014). Several studies are done regarding climate change impacts in Ethiopia. Among them, the hydrological response to climate change in the Bilate catchment, Ethiopia was assessed, and the outcomes showed that the temperature and evapotranspiration (ET) are expected to rise, while runoff, groundwater, and water yield are projected to decline in the watershed (Kuma *et al.* 2021). Similarly, the effect of climate change on streamflow in the Gelana watershed, Rift valley basin, Ethiopia was evaluated, and the results revealed that the temperatures and ET were predicted to increase. These changes translate to possible reductions in the mean annual rainfall and streamflow, with a consequent higher decline of surface runoff, groundwater, and water yield. Moreover, the rainfall and streamflow are expected to face a higher decline in wet seasons (Daniel & Abate 2022).

According to the study by Dero *et al.* (2021), the land use land cover change was increased for settlement, bare land, and croplands in the upper Deme watershed. But, water body, forest, and grassland were decreased in the upper watershed in the period of 1986–2019. Besides, during these periods, high percentages of other land use and landcover in the upper Deme watershed were changed into settlement areas. This demonstrates that the urbanization causes a change in social, economic, land use land cover, and watershed management activities in the watershed. Moreover, in the Deme watershed, the society lives in rural areas, and is highly dependent on agricultural activities, and water demand and irrigation are increasing due to some investors and organizations. These activities coupled with the future global warming may result in water stress in the

watershed. Besides, the local stakeholders and farmers have not had a good understanding of the climate variability impacts at a relevant scale until now. Therefore, this study tries to address the hydrological response to climate change in Deme Watershed, Omo-Gibe Basin, Ethiopia.

2. MATERIALS AND METHODS

2.1. Study area

Deme watershed is one of the tributaries in the Omo-Gibe Basin and contributes a high amount of flow for the Gibe IV watershed, where the Koyisha hydropower project is present. It is located in the Southern part of Ethiopia in the Wolaita Zone, Sodo Zuria, and Ofa Woreda. It is bordered between Wolaita, Gamo, and Gofa Zones with a drainage area of about 1,287.9 km^2. It is a perennial river. The watershed is surrounded between 06°18′N and 06°55′N latitude and 37°22′E and 37°45′E longitude as shown in Figure 1. Rainfall in the Deme watershed has strongly varied in season and elevation. The rainfall pattern is bimodal. The wet months are extending from April to May, and August to September. The mean annual rainfall of the Deme watershed is computed to be 1,341 mm. The elevation of the Deme watershed ranges from 1,138 to 3,269 m above sea level. In addition, the climatic condition of the Deme watershed ranges from humid to semi-arid regions.

2.2. Data collection, purposes and analysis

The spatial data (DEM) of Deme watershed of (12.5 m × 12.5 m resolution) were downloaded from Alaska satellite facility (https://asf.alaska.edu/) and used to delineate the watershed, and calculate the sub-basins parameters. Then, the soil map and land use/land cover map data obtained from Ethiopia Ministry of Water, Irrigation, and Energy (MoWIE) were added into SWAT and we classified the slope to create the Hydrological Response Unit (HRU) based on their homogeneity.

Next, the collected input data from institutions, such as climate data (maximum and minimum temperature, rainfall, relative humidity, wind speed, solar radiation) from 1987 to 2019 were collected from the Ethiopian National Meteorological Agency. The Average and Normal ratio methods were used to fill the missing meteorological data records, because of their computational simplicity and significant precisions. Double Mass Curve analysis was used for checking the consistency of recorded data. Homogeneity of the selected stations rainfall records was checked by the non-dimensional parameterization method. The streamflow data are necessary for calibration and validation of the SWAT model and are used to evaluate the streamflow response to climate change. The Deme streamflow was gauged at Oreta-Alem station and data from 1987 to 2010 was collected from the Ministry of Water and Energy. This station was used for calibration and validation of the hydrological model (SWAT).

In addition, the climate data were used by downscaling the output of the RACMO22T-RCM using CORDEX-Africa under RCP4.5 and RCP8.5 emission scenarios for the base period (1991–2010), and future periods (2031–2070). The climate variables were extracted from CORDEX-Africa Regional Climate Model (RCM) output by using Arc-GIS to the study area by considering the meteorological data gauging stations' latitude and longitude coordinates.

Further, the biases of RCM simulations were adjusted comparatively with historical observed data by using Distribution Mapping (DM) of Precipitation for precipitation, and Variance Scaling (VARI) of Temperature for temperature correction. Moreover, the performances of the selected RCM and bias correction method were evaluated by using the statistical indicators techniques. Then, the climate variables such as maximum and minimum temperature, and precipitation were projected for future periods (2031–2050 and 2051–2070) under RCP4.5 and RCP8.5 scenarios.

After that, the sensitivity analysis, calibration, validation, and uncertainty analysis of the SWAT model were done by SUFI-2 embedded in the SWAT-CUP, and its performance was evaluated by using the statistical indicators.

Finally, the streamflow was simulated for future periods under RCP4.5 and RCP8.5 scenarios by using the SWAT model. Moreover, the climate change effect on surface runoff, groundwater, total water yield, potential evapotranspiration (PET) and actual ET were evaluated. Similarly, the climate change impact in monthly, seasonal, and annual streamflow for future periods relatively with baseline period were evaluated.

According to the land use/land cover classification, seven major land uses and land cover types were identified in the Deme watershed. The classes are coded by four letters according to the SWAT database as Agricultural land (AGRL), Shrubland (RNGB), Bareland (BARR), Forest-mixed (FRST), Settlement (URBN), Grass land (PAST), and Water bodies (WATR). The SWAT model requires a basic physical–chemical property of the soil types (Dibaba *et al.* 2020). Its simulation depends on the soil data to determine the variety of hydrological characteristics found in each sub-basin within the watershed. The soil map of the study area was extracted using the Deme watershed shape file. The soil types of the study area were classified into three major groups. These are Eutric Cambisols, Eutric Nitosols, and Ochric Andosols.

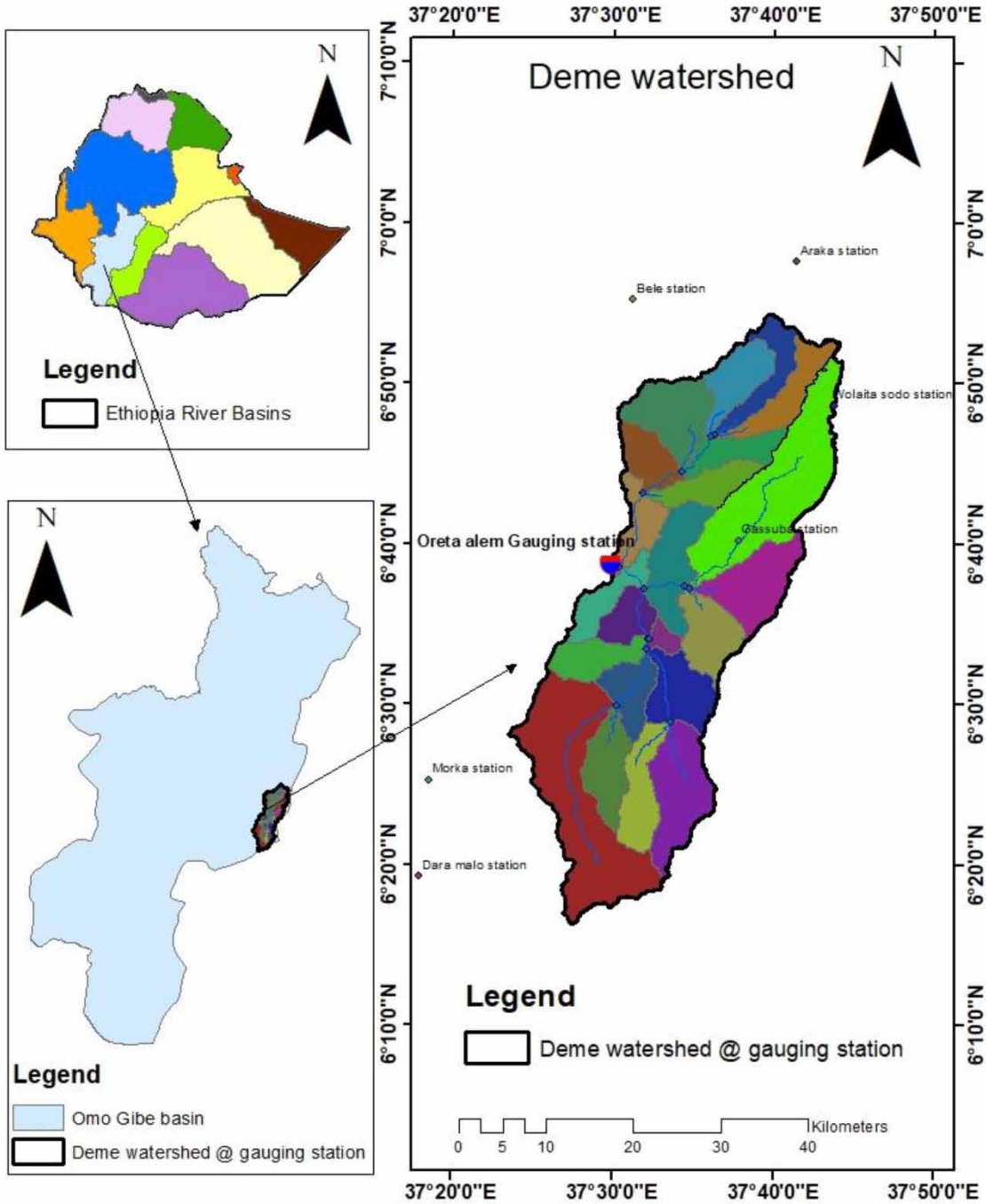

Figure 1 | Location map of the Deme watershed, meteorological and stream flow gauging stations.

2.3. Observed meteorological data

There are six meteorological stations in and around the Deme watershed as shown in Table 1.

2.4. Materials used

The data were successfully analyzed by using the different materials and software. Arc-GIS 10.4.2 was used to obtain the spatial information of the watershed, to generate the climate data from the RACMO22T climate model to the Deme watershed. The Arc-SWAT 2012 model was used to delineate the Deme watershed, assess the water balance components, and

Table 1 | Meteorological data and the locations in the Deme watershed

Station names	Latitude	Longitude	Elevation	Data length
Bele	6.92	37.52	1,240	1987–2019
Areka	6.96	37.69	1,752	1987–2019
Dara Malo	6.32	37.30	1,182	1987–2019
Gessuba	6.67	37.63	1,650	1987–2019
Morka	6.42	37.31	1,221	1987–2019
Wolaita sodo	6.81	37.73	1,854	1987–2019

simulate the current and future periods streamflow. SWAT-CUP 2012 was used to analyze the sensitivity, calibration, validation, and uncertainty of the Arc-SWAT 2012 model. Google Earth was used to obtain and check the coordinate and elevation data, and provides a view of the watershed. Climate model data for hydrologic modeling (CMhyd) software were used to extract and correct the bias of climate data (precipitation, temperatures) obtained from RACMO22T RACMO22T. The homogeneity of the hydrological data (Deme stream flow) was checked by RAINBOW software. PCPSTAT and DEW02 were used to prepare the weather data generator algorithm for the SWAT model.

2.5. General framework of the study

The general framework of the study to achieve the objective is shown in Figure 2.

2.6. Climate model data extraction

The modeling approach and the resolution of the model vary from one model type to another. The climate models driven by Global Climate Model (GCM) projections can limit the exact simulations of regional climatology owing to the inability to accurately simulate features of local or regional climate including topography, orthography, cloudiness, and land use due to the inherent coarse spatial resolution ranging between 100 and 250 km. Whereas, the resolution of RCMs is tens of kilometers, in the range of 12–50 km, in the proximity of the watershed scale. The RCM is also called the limited-area model (Dibaba *et al.* 2019; Gunathilake *et al.* 2020).

The downscaled RCM data were obtained from https://esgf-data.dkrz.de/search/cordex-dkrz. The CORDEX-Africa model data at longitude 0.44° and latitude 0.44° horizontal resolution and a multi-model ensemble of regional climate models with their driving GCMs provided the boundary conditions (Kuma *et al.* 2021). Africa was nominated as the target area of CORDEX for three main reasons. These are: the high vulnerability to climate changeability, relatively low adaptive capacity of its economies, and substantial changes in rainfall and temperature patterns (Giorgi *et al.* 2009).

The major driving forces for future expansion of greenhouse gas emissions of substances are technological innovation, energy choice, socioeconomic and demographic growth, and their integrations (Daniel & Abate 2022). According to a classification by Van Vuuren *et al.* (2011), the Representative concentration pathways, RCP4.5 and RCP8.5 scenarios were used for the study. Moreover, among the several RCMs, based on the vintage, resolution, validity, and representativeness, the RACMO22T model was selected, which was endorsed by Dibaba *et al.* (2019); and Daniel & Abate (2022). The RACMO22T model data of precipitation, maximum and minimum temperatures were extracted by Arc-GIS 10.4.1 software through a multidimensional tool and NetCDF table view. The grid points data were extracted, which are the nearest for observed meteorological stations by using the latitude and longitude of observed stations.

2.7. Bias correction methods

2.7.1. Climate model data for hydrologic modeling (CMhyd) software

CMhyd software was obtained from https://swat.tamu.edu/software/. It was used to correct the bias of precipitation, minimum and maximum temperature simulation for historical (1991–2010) and future periods (2031–2070) of analysis under both RCP4.5 and RCP8.5 scenarios.

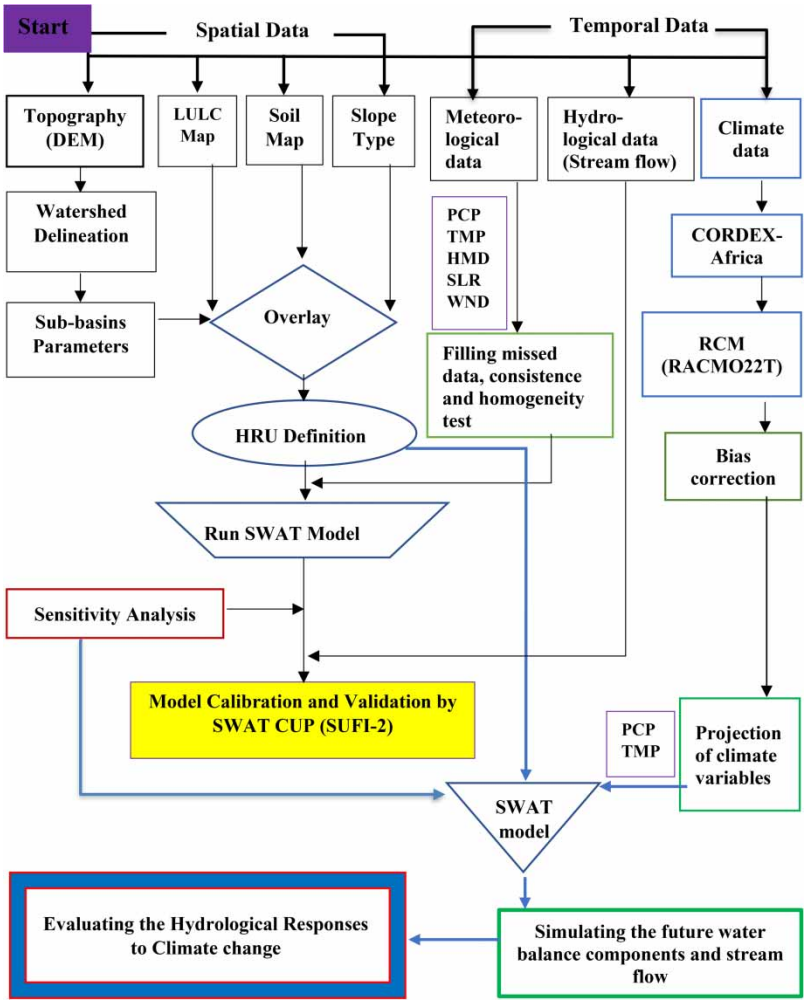

Figure 2 | The general framework of the study. PCP indicates precipitation, TMP indicates temperature, HMD indicates relative humidity, SLR indicates solar radiation, and WND indicates wind speed.

2.7.2. Precipitation correction

2.7.2.1. DM of precipitation. The DM method is applied to correct the distribution function of the RCM outputs and to align them with the observed distribution function. This can be done by creating a transfer function to shift the occurrence distributions of precipitation. It is based on the assumption that both the RCM-simulated and observed climatic variables obey a specific frequency distribution (Teutschbein & Seibert 2012). The DM method uses the transferring of function to adjust the cumulative distribution of estimated data to the cumulative distribution of rain gauges, and it reproduces precipitation very well (Dibaba *et al.* 2020; Daniel & Abate 2022).

The Gamma distribution with shape parameter α and scale parameter β is often considered to be appropriate for a precipitation probability distribution, which previous studies have shown to be effective (Zhang *et al.* 2018).

$$f_\gamma(x\,|\alpha,\,\beta) = x^{\alpha-1}\frac{1}{\beta^\alpha \times \Gamma(\alpha)} \times e^{\frac{-x}{\beta}};\ x \geq 0;\ \alpha,\,\beta > 0 \tag{1}$$

where (Γ) is the Gamma function; α and β are the form and scale parameters, respectively.

2.7.2.2. Local intensity scaling (LOCI) method for precipitation. The LOCI method aims to simultaneously correct the precipitation intensity and frequency. Initially, the rainfall intensity threshold for each month is confirmed. Accordingly,

the number of wet days in RCM precipitation that exceed this threshold matches the number of days for which observed precipitation is determined. This approach can effectively eliminate the drizzle effect because too many drizzly days are often included in original RCM outputs (Luo *et al.* 2018).

A scaling factor is calculated to ensure that the mean amounts of corrected precipitation are equal to observations

$$\left(\frac{\mu\left(P_{obs,m,d} \mid P_{obs,m,d} > 0\right)}{\mu\left(P_{his,m,d} \mid P_{his,m,d} > P_{thres,m}\right)}\right) \tag{2}$$

$$S_m = \frac{\mu\left(P_{obs,m,d} \mid P_{obs,m,d} > 0\right)}{\mu\left(P_{his,m,d} \mid P_{his,m,d} > P_{thres,m}\right)} \tag{3}$$

$$P_{hst,m,d}^{cor} = \begin{cases} P_{hst,m,d} \times S_m & P_{hst,m,d} > P_{thres,m} \\ 0 & P_{hst,m,d} < P_{thres,m} \end{cases} \tag{4}$$

where $P^{cor}{}_{hst,m,d}$ denotes the corrected precipitation on the dth day of the mth month; $P_{hst,m,d}$ denotes the precipitation from the original RCM outputs during the relevant period; $P_{obs,m}$ denotes the observed precipitation in the corresponding month during the control period; the subscripts d and m are specific days and months, respectively, and μ denotes the mean value.

The specific threshold used to define a wet day in the LOCI method is applied prior to the DM method.

$$P_{hst,m,d}^{corr} = F_{\gamma}^{-1}(F_{\gamma}(P_{LOCI,hst,m,d} \mid \alpha_{LOCI,hst,m}, \beta_{LOCI,hst,m}) \mid \alpha_{obs,m}, \beta_{obs,m}) \tag{5}$$

where F_{γ} and F_{γ}^{-1}, respectively, represent the Gamma cumulative distribution functions (cdfs) and their inverse, $P^{cor}{}_{hst,m,d}$ denotes the corrected precipitation on the dth day of the mth month; $P_{LOCI,\ hst,m,d}$ denotes the wet day precipitation on the dth day of the mth month; the subscripts d and m are specific days and months, respectively, α and β denote shape parameter and scale parameter, respectively, *obs* indicates observed, and *his* indicates historical.

2.7.3. Temperature correction

2.7.3.1. VARI of temperature. VARI of the temperature method is developed to correct both the mean and variance of temperature (Luo *et al.* 2018).

There are three steps. The mean corrected results instituted by the linear scaling approach are further normalized upon a monthly basis to a zero mean.

$$T_{hst,m,d} = T_{LS,hst,m,d} - \mu\left(T_{LS,hst,m}\right) \tag{6}$$

The standard deviation (σ) of the normalized time series is then corrected in accordance with the ratio of the observed σ and the normalized series σ, as shown in the following equation.

$$\sigma_{hst,m,d} = T_{hst,m,d} \times \frac{\sigma_m(T_{obs,m,d})}{\sigma_m(T_{hst,m,d})} \tag{7}$$

Then, the corrected temperature is calculated in accordance with the corrected μ and σ.

$$T_{hst,m,d}^{corr} = \sigma_{hst,m,d} + \mu\left(T_{LS,hst,m}\right) \tag{8}$$

2.8. Performance evaluation of climate model and bias correction methods

There are some pre-requisites for the selection of climate model and bias correction methods. In addition, their performances were evaluated by using statistical indicators. The performance of the selected RCM and bias correction methods were evaluated using four approaches: Pearson correlation coefficient (R), Root Mean Square Error (*RMSE*), Nash–Sutcliffe Efficiency (*NSE*), and Percent bias (*PBIAS*).

Pearson correlation coefficient is a measure of the strength of the relationship between model simulations and observations, and it has the limits of 1 and −1, where 1 indicates a perfect positive correlation between model and observed data, while −1 indicates a perfect negative correlation between the two (Dibaba *et al.* 2019; Daniel & Abate 2022). A value of greater than

0.5 is typically taken as satisfactory.

$$R = \frac{\sum_{i=1}^{n} ((RCM_i - RCM_{avg}) \times (OBS_i - OBS_{avg}))}{\sqrt{\sum_{i=1}^{n} (RCM_i - RCM_{avg})^2 \sum_{i=1}^{n} (OBS_i - OBS_{avg})^2}} \quad (9)$$

RMSE is a measure of the absolute error of the climate model in simulating certain climate variables. The smaller the *RMSE*, the better the model and vice versa (Dibaba *et al.* 2019; Daniel & Abate 2022).

$$RMSE = \sqrt{\frac{1}{N} \sum_{i=1}^{n} (RCM_i - OBS_i)^2} \quad (10)$$

NSE indicates how well the simulation matches the observation, and it ranges between $-\infty$ and 1, with $NSE = 1$ meaning a perfect fit. The higher this value, the more reliable, and the model is in comparison to the mean (Fang *et al.* 2015).

$$NSE = 1 - \frac{\sum_{i=1}^{n} (OBS_i - RCM_i)^2}{\sum_{i=1}^{n} (OBS_i - OBS_{avg})^2} \quad (11)$$

PBIAS measures the average tendency of the simulated data to their observed counterparts. Positive values indicate underestimation while negative values indicate overestimation by the climate model. The optimal value of PBIAS is 0.0, with low-magnitude values indicating accurate model simulations (Fang *et al.* 2015; Daniel & Abate 2022).

$$PBIAS = \frac{\sum_{i=1}^{n} (OBS_i - RCM_i)}{\sum_{i=1}^{n} OBS_i} \quad (12)$$

where *RCM* is simulated values, *OBS* is observed values, RCM_{avg} and OBS_{avg} are the corresponding average values for simulated and observed variables, respectively, *i* refers to the simulated and observed pairs at a particular period, and *N* is the total number of such pair.

2.9. Hydrologic modeling using SWAT

The Soil and Water Assessment Tool (SWAT) is a model that simulates the hydrology of the watershed. It is a deterministic hydrologic model, and it is the semi-distributed model. It was developed in the early 1990s by the Agricultural Research Service of the United States Department of Agriculture (Neitsch *et al.* 2002). The study-dependent factors to select the SWAT model are as follows:

- It is physically based.
- It uses readily available inputs.
- The model is computationally efficient and simulates the major hydrological process in the catchments.
- It is continuous in time and capable of simulating for long periods.
- The model is verified by numerous studies for the assessment of climate change on the hydrological cycles in different parts of the world.
- It is an easily available model.

2.9.1. Hydrologic water balance

The water balance is the driving force behind the entire watershed hydrologic cycle. The hydrologic cycle simulated by SWAT is based on the following water balance equation:

$$SW_t = SW_o + \sum_{t=1}^{t} (R_{\text{day}} - Q_{\text{surf}} - E_a - W_{\text{deep}} - Q_{gw}) \tag{13}$$

where SW_t is the final soil water content in mm, SW_o is the initial soil water content in a day in mm, t is the time in days, R_{day} is the amount of precipitation in a day in mm, Q_{surf} is the amount of surface runoff in a day in mm, E_a is the amount of evapotranspiration in a day in mm, W_{deep} is the amount of water entering the vadose from the soil profile in a day (mm), and Q_{gw} is the amount of the return flow in a day in mm.

2.9.2. SWAT simulation

The SWAT model simulation of the routing phase of the hydrological cycle can be explained as the movement of water over the channel network of the watershed to the outlet. The SWAT input files were organized and the model was set to run, at the end, it simulates. Daily climate data such as rainfall, temperature (maximum and minimum temperature), solar radiation, wind speed, and relative humidity were required for the SWAT modeling. The 24 years including 2-year warm-up period of the six meteorological stations (Wolaita sodo, Gessuba, Morka, Dara malo, Areka, and Bele stations) from January 1, 1987 to December 31, 2010 were used for SWAT simulation depending on data availability.

2.9.3. Estimation of surface runoff

The SWAT model uses the concept of infiltration excess runoff mechanism and it assumes the runoff comes about when the rainfall intensity is more than the infiltration rate. This phenomenon happens in areas with significant soil erosion that occurs during very high rainfall intensity storm events in the irrigated field and urban areas (Shiferaw *et al.* 2018). For this research, the Soil Conservation Services (SCS) curve number was used to estimate the surface runoff due to its capability to use daily input data.

The SCS runoff equation is an empirical model that came into common use in the 1950s. The model was developed to provide a consistent basis for estimating the amounts of runoff under varying land use and soil types.

The SCS curve number equation is:

$$Q_{\text{surf}} = \frac{(R_{\text{day}} - I_a)^2}{R_{\text{day}} - I_a + S} \tag{14}$$

where Q_{surf} is the accumulated runoff or rainfall excess (mm H_2O), R_{day} is the rainfall depth for the day (mm H_2O), I_a is the initial abstractions which include surface storage, interception, and infiltration prior to runoff (mm H_2O), and S is the retention parameter (mm H_2O).

Thus, a runoff will only occur when $R_{\text{day}} > I_a$. The curve number is mainly determined based on the soil type and land uses/land cover in the watershed. The retention parameter varies spatially due to changes in soils, land use, management, and slope, and temporally due to changes in soil water content. The retention parameter is defined as:

$$S = 25.4 \left(\frac{100}{CN} - 10 \right) \tag{15}$$

where CN is the curve number for the day.

The initial abstractions, I_a is commonly approximated as $0.2S$. Finally, the SCS curve number equation becomes:

$$Q_{surf} = \frac{(R_{day} - 0.2S)^2}{R_{day} + 0.8S} \tag{16}$$

2.9.4. Calculation of the peak runoff rate

SWAT calculates the peak runoff rate with a modified rational method. The rational method assumed that precipitation of intensity, I, begins at time $t = 0$ and continues indefinitely, while the rate of runoff will increase until the time of concentration, $t = t_{conc}$.

The modified rational method is mathematically expressed in Equation (17):

$$q_{\text{peak}} = \frac{\alpha_{tc} \times Q_{\text{surf}} \times A}{3.6 \times t_{\text{conc}}} \tag{17}$$

where q_{peak} is the peak runoff rate (m^3/s), α_{tc} is the fraction of daily precipitation that occurs during the time of concentration, Q_{surf} is the surface runoff (mm), A is the sub-basin area (km^2), t_{conc} is the time of concentration (h), and 3.6 is a conversion factor.

2.9.5. Sensitivity analysis, calibration, and validation of SWAT model

Sequential Uncertainty Fitting version 2 (SUFI-2) was embedded in the Arc-SWAT-CUP, which was used for the sensitivity analysis, calibration, and validation of the SWAT model. This algorithm was found to be quite effective (Abbaspour *et al.* 2015).

The SUFI-2 was given several iterations to reach acceptable results. Each iteration provides the suggested values for the new parameters to be used in the next iteration. Until the best fit curve of simulated versus observed streamflow data was obtained, the sensitive parameters were changed again and again in the allowable range recommended by SWAT-CUP. Finally, it achieved an acceptable result with the values of the Nash–Sutcliffe, Coefficient of determination, Percent of bias, and other uncertainty analysis statistical parameters. The sensitivity parameters were identified with their ranges which is necessary to reduce the computational time required for SWAT model calibration. This process is called sensitivity analysis. All SWAT model parameters involved in the hydrological process were reduced into the most sensitive parameters with different degrees of sensitivity based on a low P-value and a high absolute value of t-Stat (Dibaba *et al.* 2020; Daniel & Abate 2022).

Calibration is the determination to better parameterize a model to a given set of local conditions, through comparing the model prediction with the observed data, thus reducing the prediction uncertainty (Arnold *et al.* 2012). Calibration was done next to identifying the sensitive parameters by comparing model-simulated streamflow with observed streamflow data from the period of January 1, 1989 to December 31, 2000.

To utilize the calibrated model for estimating the effectiveness of future potential management practices, the model should be tested against an independent set of measured data without further adjustments; this testing of a model with an independent data set is commonly referred to as model validation (Dibaba *et al.* 2020). It is the final step of the hydrologic modeling, verifying the performance of the SWAT model for simulated flows in periods different than the calibration periods of January 2001 to December 2010. Generally, the objective function used in SWAT-CUP (SUFI-2) for calibration and validation of the SWAT model was NSE in this study. Because it is very commonly used, the best objective function for reflecting the overall fit of a hydrograph provides extensive information, and it is less sensitive to high extreme values due to the squared differences (Moriasi *et al.* 2007).

2.9.6. SWAT model performance evaluation

Statistics techniques such as coefficient of determination, NSE, and PBIAS were used to express the good fitness of the model simulation with the observed streamflow (Daniel & Abate 2022).

Coefficient of determination (R^2) indicates how the simulated data correlates to the observed values of the data. R^2 ranges from 0 to 1, with higher values indicating less error variance, and typically values greater than 0.5 are considered acceptable. This statistic is oversensitive to high extreme values (outliers) and insensitive to additive and proportional differences between model predictions and measured data (Moriasi *et al.* 2007).

$$R^2 = \frac{\sum_{i=1}^{n} [(O_i - O_{\text{avg}})(S_i - S_{\text{avg}})]^2}{\sqrt{\sum_{i=1}^{n} (O_i - O_{\text{avg}})^2 \sum_{i=1}^{n} (S_i - S_{\text{avg}})^2}} \tag{18}$$

where R^2 is the coefficient of determination, O_i is the ith observed parameter, O_{avg} is the mean of the observed parameters, S_i is the ith simulated parameter, S_{avg} is the mean of model-simulated parameters, and n is the total number of events.

NSE is very commonly used, and provides extensive information on reported values. It measures how well trends in the observed data are reproduced by the simulated results over a specified period and for a specified time step. It is also the best objective function for reflecting the overall fit of a hydrograph. It is less sensitive to high extreme values due to the squared differences. It indicates how well the plot of observed versus simulated data fits the 1:1 line. NSE ranges between $-\infty$ and 1 (1 inclusive), with NSE = 1 being the optimal value. Values between 0 and 1 are generally viewed as acceptable levels of performance, whereas values of NSE $\leq$ 0 indicate unacceptable performance (Moriasi *et al.* 2007).

$$NSE = 1 - \frac{\sum_{i=1}^{n} (O_i - S_i)^2}{\sum_{i=1}^{n} (O_i - O_{\text{avg}})^2} \tag{19}$$

where *NSE* is the Nash–Sutcliffe Efficiency coefficient, O_i is the *i*th observed parameter, O_{avg} is the mean of the observed parameters, S_i is the *i*th simulated parameter, and n is the total number of events.

PBIAS measures the mean tendency of the simulated data to be larger or smaller than their observed counterparts. Its values for streamflow tend to vary more among different autocalibration methods during dry years than during wet years. This fact should be considered when attempting to do a split sample evaluation, one for calibration and one for validation (Moriasi *et al.* 2007). The optimal value of PBIAS is 0, with low-magnitude values indicating accurate model simulation. Positive values indicate model underestimation bias, and negative values indicate model overestimation.

$$PBIAS = \frac{\sum_{i=1}^{n} O_i - \sum_{i=1}^{n} S_i}{\sum_{i=1}^{n} O_i} \times 100 \tag{20}$$

where *PBIAS* is the percent bias, O_i is the *i*th observed parameter, S_i is the *i*th simulated parameter, and n is the total number of events.

2.9.7. Uncertainty analysis of the SWAT model

SWAT parameters account for foundations of uncertainties, for instance, uncertainty in driving variables, conceptual models, parameters, and measured data. Uncertainty analysis measures the goodness of fit and the 95% prediction uncertainty between simulated and observed streamflow (Abbaspour *et al.* 2015). The p-factor and r-factor statistics were considered to quantify the fit between the result expressed as 95PPU and observation. The degree of uncertainties was measured as the p-factor, which is the percentage of observed data related by the 95PPU (95% prediction uncertainty). The 95PPU is calculated by the 2.5 and 97.5% levels of the cumulative distribution of the output variables. Moreover, the measure quantifying the strength of uncertainty analysis was the *r*-factor, which is the average thickness of the 95PPU band ($\bar{r}$) divided by the standard deviation of the measured data as described in Equations (21) and (22). The *p*-factor, i.e., the percentage of observations covered by the 95PPU, varies from 0 to 1 with the ideal value of 1, while for the *r*-factor, the thickness of the 95PPU optimal value is around 1 (Dibaba *et al.* 2020; Daniel & Abate 2022).

$$\bar{r} = \frac{1}{n} \sum_{t_i}^{n} (y_{t_i}^{M},\ 97.5\,\% - y_{t_i}^{M},\ 2.5\,\%) \tag{21}$$

$$r - \text{factor} = \frac{p - \text{factor}}{\sigma_{obs}} \tag{22}$$

where $y^M t_i$, 97.5% and $y^M t_i$, 2.5% represents the upper and lower boundaries of the 95PPU, and σ_{obs} is the standard deviation of the measured data.

2.10. Potential evapotranspiration

PET is determined primarily by net radiation and temperature, but also by the moisture-holding capacity of the air and other factors. Increasing temperature will lead to more evaporation, although the effect is complicated and alters the hydrologic

regime in and around the catchment. Climate change manifests itself through increasing temperatures that lead to an increase in actual ET, which will accelerate the hydrological cycle (Jiménez *et al.* 2014).

In the SWAT model there are options for estimating PET, though, the Penman-Monteith method is endorsed for determining reference ET, when the standard meteorological data have temperature, relative humidity and sunshine hours (Daniel & Abate 2022). Hence, PET was calculated by the FAO Penman–Monteith method. The Penman–Monteith equation

$$ET_O = \frac{0.4080\ \Delta(R_n - G) + \gamma \frac{900}{T+273} U_2\ (e_s - e_a)}{\Delta + \gamma(1 + 0.34\ U_2)} \tag{23}$$

where ET_O is the reference evapotranspiration (mm day^{-1}), R_n is the net radiation at the crop surface (MJ m^{-2} day^{-1}), G is the soil heat flux density (MJ m^{-2} day^{-1}), T is the mean daily air temperature at 2 m height (°C), U_2 is the wind speed at 2 m height (m s^{-1}), e_s is the saturation vapor pressure (kPa), e_a is the actual vapor pressure (kPa), e_s–e_a is the saturation vapor pressure deficit (kPa), Δ is the slope vapor pressure curve (kPa °C^{-1}) and γ is the psychrometric constant (kPa °C^{-1}).

3. RESULTS AND DISCUSSION

3.1. Sensitivity analysis, calibration, validation, and performance of the SWAT model

3.1.1. Sensitivity analysis

The most sensitive parameters which affect the SWAT model output were evaluated by using the SWAT-CUP (SUFI-2). The small valued sensitivity parameters do not expressly affect the hydrological model output. Nevertheless, from medium to very high ranked sensitive parameters that significantly affect the SWAT model output were used to calibrate and validate the model. The result of SWAT sensitivity analysis, ranges, and their fitted values in the Deme watershed at Oreta-Alem gauging station are tabulated in Table 2. It indicates ALPHA_BF.gw (Baseflow alpha factor in days), CH_K2.rte (Effective hydraulic conductivity in main channel alluvium), RCHRG_DP.gw (Deep aquifer percolation fraction), ESCO.hru (Soil evaporation

Table 2 | Sensitivity ranks of parameters for SWAT model calibration

Parameter name	Sensitivity			Absolute SWAT values	Calibration
	Sensitivity rank	t-Stat	*p*-value	Range	Fitted value
V__ALPHA_BF.gw	1	6.16	0.00	0–1	0.0001
V__CH_K2.rte	2	−5.29	0.00	−0.01–500	36.25
V__RCHRG_DP.gw	3	2.34	0.02	0–1	0.68
V__ESCO.hru	4	−1.90	0.06	0–1	0.05
R__SLSUBBSN.hru	5	−1.84	0.07	10–150	−0.11
V__GWQMN.gw	6	−1.71	0.09	0–5,000	2,298.75
V__REVAPMN.gw	7	−1.65	0.10	0–500	70.79
R__BIOMIX.mgt	8	1.54	0.12	0–1	0.47
V__GW_REVAP.gw	9	−1.12	0.26	0.02–0.2	0.19
V__HRU_SLP.hru	10	−0.84	0.40	0–1	0.23
R__CH_N2.rte	11	0.75	0.45	−0.01–0.3	−0.20
R__CN2.mgt	12	0.69	0.49	35–98	−0.30
V__GW_DELAY.gw	13	−0.49	0.63	0–500	34.63
R__SOL_K(..).sol	14	0.32	0.75	0–2,000	−0.41
V__EPCO.hru	15	0.31	0.76	0–1	0.56
R__SOL_Z(..).sol	16	−0.20	0.84	0–3,500	0.15
R__SOL_AWC(..).sol	17	−0.13	0.90	0–1	0.05
V__OV_N.hru	18	−0.09	0.93	0.01–1	0.39

Note: R-means an existing parameter value is multiplied by (1 + *a* fitted value), V-means an existing parameter value is to be replaced by a fitted value.

compensation factor), SLSUBBSN.hru (Average slope length), GWQMN.gw (Threshold depth of water in the shallow aquifer required for return flow to occur in mm were found to be the six topmost sensitive parameters at the Oreta-Alem gauging station in the Deme watershed.

3.1.2. Flow calibration and validation

The selected 18 sensitive parameters were used for calibration and validation of the SWAT model with SWAT-CUP (SUFI-2) on monthly time steps from 1989 to 2010. From the total continuous time series, flow gauging periods from 1989 to 2000 were selected as the calibration period, and the remaining periods, i.e., from 2001 to 2010, were used for validation of the hydrological model. Moreover, the SWAT model calibration and validation are shown in Figure 3.

3.1.3. Hydrological model performances

The calibration results on mean monthly flow show that the SWAT model can capture the observed streamflow with R^2, *NSE*, and *PBIAS* of 0.77, 0.73, and 4.6, respectively. The average monthly flow validation indicates R^2, *NSE*, and *PBIAS* of 0.82, 0.75, and 14.2, respectively. Generally, the hydrological model showed a reasonably good agreement in the Oreta-Alem gauging station. Hence, according to descriptions by Moriasi *et al.* (2007), the SWAT model has an acceptable performance in the Deme watershed.

3.2. Performance of bias correction methods and climate model

The bias of RACMO22T (RACMO22T) simulations was corrected by the DM for adjusting the precipitation, and VS of temperature were used for adjusting the maximum and minimum temperature.

Generally, the DM method for precipitation and VS method for maximum and minimum temperature bias correction showed very good performance as tabulated in Table 3, and were used to adjust the climate variables of future periods. The related conclusion was reported by Daniel & Abate (2022). Also, it is supported by Geleta & Gobosho (2018) and Dibaba *et al.* (2020), in the Finchaa watershed in Ethiopia. Besides, the results revealed that the RACMO22T climate

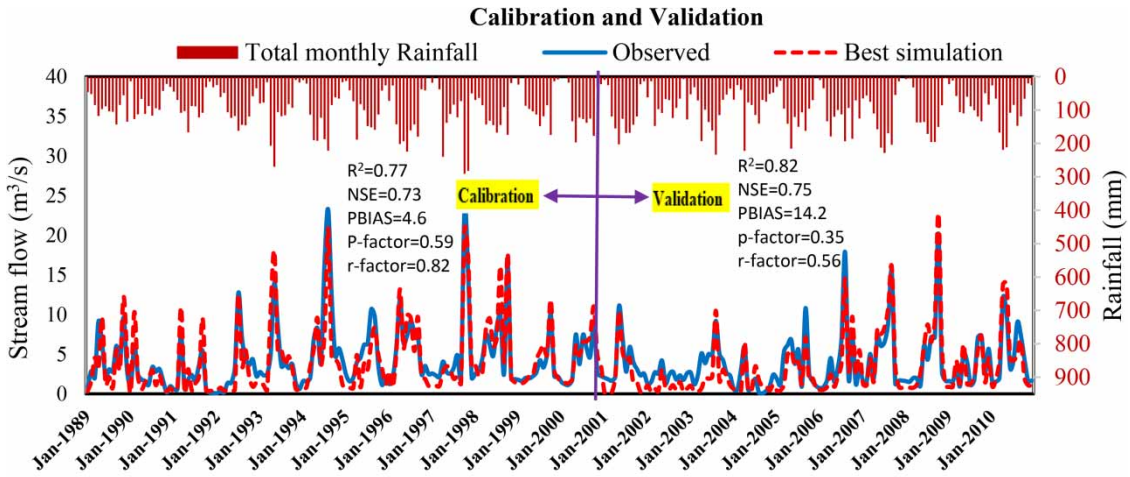

Figure 3 | Calibration and validation of average monthly streamflow.

Table 3 | Performance of bias correction methods to adjust precipitation (PCP), maximum temperature (TMAX) and minimum temperature (TMIN) in the study area

Watershed	RCM	Performance statistics	PCP DM	TMAX VS	TMIN VS
Deme	RACMO22T	PBIAS	−0.01	0.01	0.01
		R	0.99	0.99	0.98
		RMSE	0.08	0.02	0.04
		NSE	0.99	0.99	0.98

model performed better in reproducing daily precipitation, maximum, and minimum temperatures in the Deme watershed. The corresponding study was also done by Dibaba *et al.* (2019) and Daniel & Abate (2022). Thus, the RACMO22T climate model was used in the study to model climate variables.

3.3. Climate change projections

To evaluate the climate change effect, the precipitation and temperature were obtained from the RACMO22T model, then, the bias-corrected precipitation and temperature by DM and VS methods, respectively, for future periods (2031–2070), are compared to the base period datasets (1991–2010). Additionally, the hydrological responses of the watershed are investigated by computing and comparing the future water balance components such as surface runoff, groundwater flow, and total water yield. Besides, the PET and actual ET were analyzed for RCP4.5 and RCP8.5 scenarios.

3.3.1. Rainfall

The percentage of change in seasonal rainfall, i.e., winter (Bega) (December, January, and February); spring (Belg) (March, April, and May); summer (Kiremt) (June, July, and August); and autumn (Tseday) (September, October, and November) were evaluated as shown in Figure 4. The result shows a declining pattern in all seasons in the Deme watershed for future periods comparatively with the baseline period, except for the winter season. It will be expected to face higher decremental change in the spring season by 37.52% from 2051 to 2070 under the RCP4.5 scenario. The more profound changes in predicted rainfall were seen in seasonal bases compared to the annual bases in the Deme watershed. Generally, in the wet season, both RCP projections designate a higher reducing signal for future periods in the watershed. The supporting study was done by Kuma *et al.* (2021), in the Bilate watershed, and reported that it is predicted to decline in the spring and summer seasons. Likely, in the Gelana watershed, in wet seasons, all rainfall projections show a higher declining signal (Daniel & Abate 2022).

The annual declining rainfall in the two future periods under RCP4.5 and RCP8.5 scenarios is shown in Table 3. The rainfall will be declined by 30.14 and 27.6% under RCP4.5 and RCP8.5 scenarios, respectively, in the 2031–2050 period. Similarly, it will decline by 32.87 and 26.21% under RCP4.5 and RCP8.5 scenarios, respectively, in 2051–2070. The related projections were also confirmed by Dibaba *et al.* (2020) in the Finchaa sub-basin, Ethiopia, and by Daniel & Abate (2022) in the Gelana watershed, in Rift valley basin, Ethiopia.

3.3.2. Maximum and minimum temperatures

The changes in projected maximum and minimum temperatures are not only annual, but are also expected to vary seasonally, and resulted in a rising pattern in the Deme watershed for future periods as shown in Figure 5. A higher seasonal rise in maximum temperature is expected from the high emission scenario than the medium emission scenario. Likewise, the maximum rise is projected in the far future period (2051–2070) rather than the near future period (2031–2050). Generally, it will be expected to increase in all seasons with a high degree of variation with respect to a base period in the watershed.

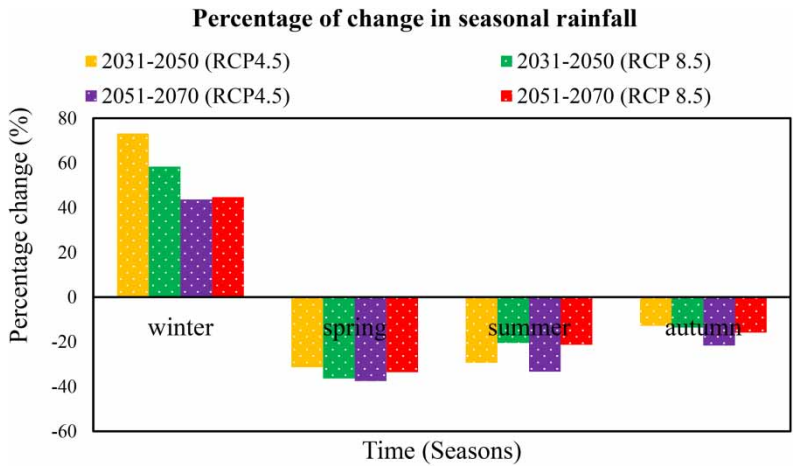

Figure 4 | The percentage of change in seasonal rainfall.

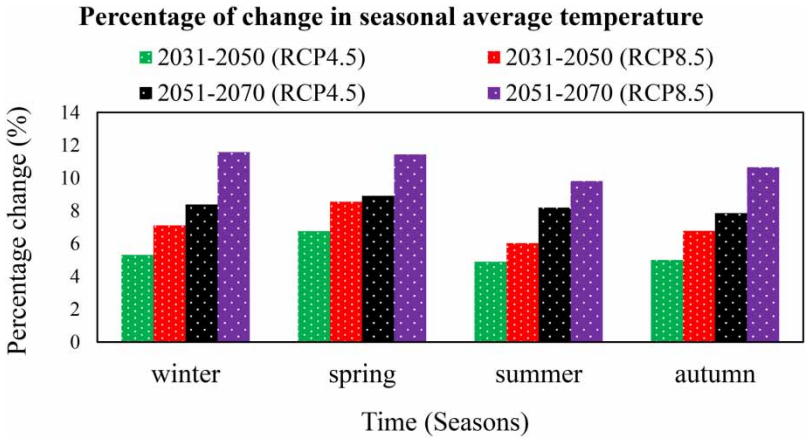

Figure 5 | The percentage of change in seasonal average temperature.

The annual maximum temperature in the Deme watershed will increase on average by 0.97 and 1.10 °C under the RCP4.5 and RCP8.5 scenarios, respectively, for the near future period. Correspondingly, an increment by 1.70 and 2.00 °C was expected under both scenarios, respectively, for the far future period with respect to the base period. Similarly, the annual minimum temperature will be increased on average by 1.19 and 1.67 °C under the RCP4.5 scenario for the near and far future periods, respectively. Likewise, it will be increased by 1.62 and 2.29 °C for the near and far future, respectively, under the RCP8.5 scenario as shown in Table 4. Moreover, the variations are higher for the minimum temperature than the maximum temperature.

The overall results indicate that maximum and minimum temperatures increase under both RCPs throughout the study years, showing the warming trends in the watershed. The highest and lowest change in temperatures under the RCP8.5 scenario is more than the RCP4.5 scenario for all time horizons, especially in the far future period concerning the baseline period. This indicates that the RCP8.5 scenario will be warmer than the RCP4.5 scenario in the Deme watershed.

Therefore, the maximum and minimum temperature predictions for future time horizons (2031–2070) under both emission scenarios are within the range confirmed by IPCC (2014). Moreover, the maximum and minimum temperatures in the Bilate watershed from 2051 to 2080 are expected to become warmer than from 2021 to 2050 under both emission scenarios (Kuma *et al.* 2021). The related study was reported by Daniel & Abate (2022) in the Gelana watershed, in Rift valley basin, Ethiopia, which concluded that the highest temperature variation with respect to the base period was seen under the RCP8.5 scenario.

3.3.3. PET and actual ET

The PET and actual ET variation between the base period (1991–2010), near future (2031–2050), and far future (2051–2070) were evaluated as shown in Table 3. The mean annual change of PET is expected to increase by 6.78 and 7.32% under both scenarios, respectively, for the near future period. Likewise, its increment is expected by 9.15 and 10.89% under both RCP scenarios, respectively, for the far future period comparatively with the base period. Furthermore, the high variation in actual ET under both RCPs was analyzed for future years. According to evaluation the actual ET will increase on average by 5.14 and 7.17% under a medium emission scenario for the near and far future periods, respectively. Likewise, it will increase by 6.34 and 9.24% for the near and far future periods, respectively, under a high emission scenario in the Deme watershed.

Table 4 | Changes in maximum and minimum temperature (°C)

	RCP4.5		RCP8.5	
	2031–2050	2051–2070	2031–2050	2051–2070
T_{min}	1.19	1.67	1.62	2.29
T_{max}	0.97	1.70	1.10	2.00

Generally, the results show that the variation rate of PET and actual ET under the RCP8.5 scenario will be more than the RCP4.5 scenario in both future time horizons due to a large increment of the maximum and minimum temperature. Moreover, the magnitude of changes will be greater in the far future than in the recent future under both emission scenarios. Therefore, changes in temperature and ET are correlated positively in the Deme watershed. Accordingly, the rise in temperature resulted in an increase in the potential and actual ET in the watershed. The increase in ET suggests increased crop water requirements in future crop production. The conforming results were done by Kuma *et al.* (2021) in the Bilate watershed, and by Daniel & Abate (2022) in the Gelana watershed, in Rift valley basin, Ethiopia.

3.4. Watershed hydrological responses to climate change

The variations in water balance components due to climate change were evaluated for future periods in Deme watershed, and the effects have resulted from the integration of rainfall, temperature, and ET with hydrological cycles. The hydrological responses of the watershed to climate changes were investigated for two future periods under the RCP4.5 and RCP8.5 scenarios. It was considered in terms of the process that contributes to the water balance components of annual surface runoff, groundwater, total water yield, PET and actual ET as shown in Table 5. The projected rainfall and temperatures for future periods from 2031 to 2070 under both RCP scenarios cause significant changes in hydrological components in the watershed.

The overall results show that the mean annual surface water runoff, groundwater, and total water yield will be expected to decrease, whereas actual ET and PET will be expected to increase in all future periods in the watershed. The maximum decline of surface runoff by 15.10%, ground water by 14.78%, and total water yield by 26.10% was seen in the near future (2031–2050) under the RCP8.5 scenario relative to the baseline period (1991–2010). These outcomes from the decreases of rainfall and increases of mean temperature, actual ET and PET led to a decline in surface runoff, groundwater, and total water yield in the Deme watershed.

The maximum rise in mean annual temperature seen by 2.15 °C in the far future period under the RCP8.5 scenario corresponded to the base period. The related study was done by Dibaba *et al.* (2020), which showed the annual mean temperature in the Finchaa watershed is projected to rise by 1.1–3.1 °C in the 2060s.

Consequently, the temperature rise resulted in increased PET and actual evaporation, which could be a critical factor for the reduction of total water yield. As the forms of water are exposed to losses, owing to the changes in temperature, the evaporation is also a factor for the future period reduction of the surface runoff and groundwater in the watershed. These indications of water shortage will be more pronounced in the future periods due to the warming of the atmosphere through climate changes. These results are consistent with the study done in the Bilate watershed by Kuma *et al.* (2021), who reported that a 15.39% decline in the rainfall resulted in around 9.22, 11.11, and 10.25% reduction in water yield, groundwater, and surface runoff, respectively, under the RCP4.5 scenario from 2051 to 2080. It is likely that a 2.0 °C increase in the mean annual temperature will lead to a rise in PET and actual evaporation by 19 and 13.9%, respectively, under the high emission scenario in 2051–2080. The corresponding study was done in the Gelana watershed by Daniel & Abate (2022), which predicted a decline of surface runoff by 22.23%, groundwater by 42.54%, and total water yield by 35.89% in 2051–2070 under the RCP4.5 scenario corresponding to the base period.

3.5. Streamflow response to climate change

Relative changes in streamflow exhibited a large uncertainty when the projected temperature and precipitation changes were used in the SWAT model (Musau *et al.* 2015). The mean seasonal changes in the streamflow for the future periods under both RCP scenarios were predicted by using the projected rainfall and temperature, and will cause a significant variation of the future streamflow of the Deme watershed. However, the other climate variables (solar radiation, relative humidity, and wind speed); and land use land cover, soil map, and slope classification that were observed in the baseline period were

Table 5 | Changes of the annual water balance under climate change

Model	Scenarios	Period	PET (%)	ET (%)	Surface Runoff (%)	Groundwater (%)	Water Yield (%)	Rainfall (%)	Mean temp. (°C)
RACMO22T	RCP4.5	2031–2050	6.78	5.14	−6.13	−8.78	−16.58	−30.14	1.08
		2051–2070	9.15	7.17	−8.22	−10.25	−16.8	−32.87	1.68
	RCP8.5	2031–2050	7.32	6.34	−15.1	−14.78	−26.1	−27.60	1.36
		2051–2070	10.89	9.24	−12.76	−10.88	−16.38	−26.21	2.15

considered a constant for the future periods. This is because varying these parameters may not have a significant influence on modeling the climate change in local hydrology (Dibaba *et al.* 2020).

The more reflective fluctuations in projected streamflow were seen in seasonal bases concerning the annual bases in the watershed. Figure 6 indicates that there is a seasonal variation on streamflow in all future scenarios with different values. A higher reduction of streamflow changes will be expected in both the wet and dry seasons except in December, January and February. Moreover, the maximum decrease of flow variation is expected in the summer season. Specifically, it will decline by a rate of 62.20% under the RCP4.5 scenario from 2051 to 2070. Similarly, in all future periods under both RCP scenarios, the streamflow shows a high decline in the spring season. While, in the winter season, it is expected there will be a higher incremental change of 66.5% from 2051 to 2070 under the RCP8.5 scenario. Altogether, similar to a rainfall pattern, a streamflow shows a decreasing signal in the wet season than the dry season in the Deme watershed. An analogous study was carried out by Daniel & Abate (2022) in the Gelana watershed, which showed that during the autumn season there was a decline in the future horizons.

Additionally, the annual changes in the streamflow for the future periods under both RCP scenarios were predicted as shown in Table 6. It suggested decreasing streamflow in the two future periods under both scenarios. The annual streamflow is expected to decline by 21.2% under RCP4.5 and 26.2% under RCP8.5 in the near future period. In the far future, it is likely to decline by 23.0% under the RCP4.5 scenario and 24.7% under the RCP8.5 scenario in the Deme river relative to the baseline period.

Generally, due to climate change, the temperature and ET are expected to increase, and the rainfall is expected to decrease in the watershed, due to the fact that the streamflow will decrease in the future periods from 2031 to 2070 with respect to the observed streamflow in baseline period from 1991 to 2010. This shows the direct relationship between temperature and ET, and the inverse relationship with rainfall and streamflow in the Deme watershed. The findings are related to the study done by Daniel & Abate (2022) in the Gelana river, which is expected to decline by 21.09% under RCP4.5 and 32.30% under RCP8.5 in the 2031–2050. Similarly, it declines by 44.14% under RCP4.5 and 24.27% under the RCP8.5 scenario in 2051–2070. Similarly, the mean annual and monthly streamflow in the future periods shows a declining trend in the four watersheds in the upper catchments of the Nzoia river basin in western Kenya (Musau *et al.* 2015).

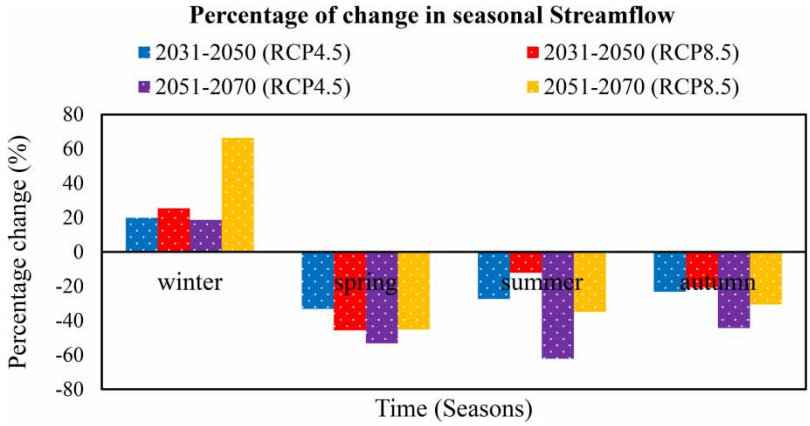

Figure 6 | Percentage change of seasonal streamflow.

Table 6 | Changes in streamflow (%)

Streamflow	RCP4.5		RCP8.5	
RCM	2031–2050	2051–2070	2031–2050	2051–2070
RACMO22T	−21.2	−23.0	−26.2	−24.7

4. CONCLUSIONS AND DIRECTIONS FOR FUTURE RESEARCH

The impact of climate change on hydro-meteorological variables has produced a significant alteration in the hydrology of the watershed. This study aims to investigate the hydrological responses to climate change in the Deme watershed using the SWAT for two consecutive periods of 2031–2050 and 2051–2070. To evaluate the hydrological responses to climate change, the precipitation and temperature were obtained from the RACMO22T model, then the bias-corrected precipitation and temperature within DM and VS methods, respectively, for future periods (2031–2070) were used for further analysis and compared to the base period datasets (1991–2010). The SWAT model was calibrated (and validated) for the 1989–2000 (2001–2010) period at the Oreta-Alem gauging station in the Deme watershed; the hydrological model showed a reasonably good agreement. The result shows a declining rainfall pattern in all seasons for future periods comparatively with the baseline period, except in the winter season. The highest seasonal rise in temperatures is expected from the high emission scenario compared to the medium emission scenario. Likewise, the maximum rise is projected in the far future period (2051–2070) compared to the near future period (2031–2050). Generally, temperatures will be expected to increase in all seasons with a high degree of variation with respect to a base period in the watershed. The more reflective fluctuations in projected streamflow were seen in seasonal bases concerning the annual bases in the watershed. Even though in the winter season there was a slight increase in the streamflow, most of the seasons in the future periods under both RCP scenarios show a declining trend relatively with an observed streamflow in the watershed. Moreover, the maximum decrease of flow variation is expected in the summer season. Specifically, it will decline by a rate of 62.20% under the RCP4.5 scenario from 2051 to 2070. Altogether, similar to rainfall patterns, the streamflow shows a decreasing trend in wet seasons rather than dry seasons in the Deme watershed. The mean annual rainfall will decline by 30.14 and 27.6% under the RCP4.5 and RCP8.5 scenarios, respectively, in the 2031–2050 period. Similarly, it will decline by 32.87 and 26.21% under the RCP4.5 and RCP8.5 scenarios, respectively, in 2051–2070.

The annual maximum temperature will increase on average by 0.97 and 1.10 °C under the RCP4.5 and RCP8.5 scenarios, respectively, for the near future period. Correspondingly, its increment was expected by 1.70 and 2.00 °C under both scenarios, respectively, for the far future period with respect to the base period. Similarly, the annual minimum temperature will increase on average by 1.19 and 1.67 °C under the RCP4.5 scenario for the near and far future periods, respectively. Likewise, it will increase by 1.62 and 2.29 °C for the near and far future, respectively, under the RCP8.5 scenario. Furthermore, the variations are higher for the minimum temperature than the maximum temperature. The overall results indicate that maximum and minimum temperatures increase under both RCPs throughout the study years, showing warming trends in the watershed. The RCP8.5 scenario will be warmer than the RCP4.5 scenario in the Deme watershed. Besides, the mean annual change of PET is expected to increase by 6.78 and 7.32% under both scenarios, respectively, for the near future period. Likewise, its increment is expected by 9.15 and 10.89% under both RCP scenarios, respectively, for the far future period compared with the base period. According to evaluation the actual ET will increase on average by 5.14 and 7.17% under the medium emission scenario for the near and far future periods, respectively. Also, it will increase by 6.34 and 9.24% for the near and far future periods, respectively, under the high emission scenario in the watershed. The overall results show that the mean annual surface water runoff, groundwater, and total water yield will be expected to decrease, whereas actual ET and PET will be expected to increase in all future periods in the watershed. The maximum decline of surface runoff by 15.10%, groundwater by 14.78%, and total water yield by 26.10% is expected in near future (2031–2050) under the RCP8.5 scenario relative to the baseline period (1991–2010). These outcomes from the decreases of rainfall and increases of mean temperature, actual ET and PET led to a decline in surface runoff, groundwater, and total water yield in the watershed. Additionally, the annual streamflow is expected to decline by 21.2% under RCP4.5 and 26.2% under RCP8.5 in the near future period. In the far future, it is likely to decline by 23.0% under the RCP4.5 scenario and 24.7% under the RCP8.5 scenario in the Deme River. Generally, due to climate change, the temperature and ET are expected to increase, and the rainfall is expected to decrease in the watershed; due to that the streamflow will decrease in the future periods from 2031 to 2070 with respect to the observed streamflow in baseline period from 1991 to 2010. This shows the direct relationship between temperature and ET, and their inverse relationship with rainfall and streamflow in the Deme watershed. Generally, the land use/land cover scenarios, and weather variables (solar radiation, windspeed, and humidity) were assumed constant for future periods during the study. However, these parameters directly contribute to hydrological systems. In future, this study should be extended by varying these parameters. Moreover, future studies should consider multiple RCMs with different scenarios for hydrological responses to climate change analysis, because it diminishes the uncertainties in climate change evaluations.

DATA AVAILABILITY STATEMENT

All relevant data are included in the paper or its Supplementary Information.

CONFLICT OF INTEREST

The authors declare there is no conflict.

REFERENCES

Abbaspour, K. C., Rouholahnejad, E., Vaghefi, S., Srinivasan, R., Yang, H. & Kløve, B. 2015 A continental-scale hydrology and water quality model for Europe: calibration and uncertainty of a high-resolution large-scale SWAT model. *Journal of Hydrology* **524**, 733–752. https://doi.org/10.1016/j.jhydrol.2015.03.027.

Arnold, J. G., Moriasi, D. N., Gassman, P. W., Abbaspour, K. C., White, M. J., Srinivasan, R., Santhi, C., Harmel, R. D., Van Griensven, A., Van Liew, M. W., Kannan, N. & Jha, M. K. 2012 SWAT: Model use, calibration, and validation. *Transactions of the Asabe* **55** (4), 1491–1508.

Biniyam, Y. & Abdella, K. 2017 The impacts of climate change on rainfall and flood frequency: the case of Hare watershed, Southern Rift Valley of Ethiopia. *Journal of Earth Science & Climatic Change* **8** (1), 1–5. https://doi.org/10.4172/2157-7617.1000383.

Chaemiso, S. E., Abebe, A. & Pingale, S. M. 2016 Assessment of the impact of climate change on surface hydrological processes using SWAT: a case study of Omo-Gibe river basin, Ethiopia. *Modeling Earth Systems and Environment* **2** (4), 1–15. https://doi.org/10.1007/s40808-016-0257-9.

Daniel, H. & Abate, B. 2022 Effect of climate change on stream flow in the Gelana watershed, Rift valley basin, Ethiopia. *Journal of Water and Climate Change* **13** (5), 2205–2232. https://doi.org/10.2166/wcc.2022.059.

Dero, K., Shiferaw, W. & Zewde, B. 2021 Urban induced land use land cover changes in upper Deme watershed, Southwest Ethiopia. *Journal of Degraded and Mining Lands Management* **9** (1), 3045.

Dibaba, W. T., Miegel, K. & Demissie, T. A. 2019 Evaluation of the CORDEX regional climate models performance in simulating climate conditions of two catchments in Upper Blue Nile Basin. *Dynamics of Atmospheres and Oceans* **87**, 101104. https://doi.org/10.1016/j.dynatmoce.2019.101104.

Dibaba, W. T., Demissie, T. A. & Miegel, K. 2020 Watershed hydrological response to combined land use/land cover and climate change in highland Ethiopia: finchaa catchment. *Water (Switzerland)* **12** (6). https://doi.org/10.3390/w12061801.

Disasa, K. N., Tura, F. S. & Fereda, M. E. 2019 Climate change downscaling using stochastic weather generator model in Rift Valley Basins of Ethiopia. *American Journal of Climate Change* **08** (04), 561–590. https://doi.org/10.4236/ajcc.2019.84030.

Fang, G. H., Yang, J., Chen, Y. N. & Zammit, C. 2015 Comparing bias correction methods in downscaling meteorological variables for a hydrologic impact study in an arid area in China. 2547–2559. https://doi.org/10.5194/hess-19-2547-2015.

Geleta, C. D. & Gobosho, L. 2018 Climate change induced temperature prediction and bias correction in Finchaa watershed. *American-Eurasian Journal of Agriculture* **18** (6), 324–337.

Giorgi, F., Jones, C. & Asrar, G. 2009 Addressing climate information needs at the regional level: the CORDEX framework. *Organization (WMO) Bulletin* **58**, 175–183.

Gunathilake, M. B., Amaratunga, Y. V., Perera, A., Chathuranika, I. M., Gunathilake, A. S. & Rathnayake, U. 2020 Evaluation of future climate and potential impact on streamflow in the Upper Nan River Basin of Northern Thailand. *Advances in Meteorology* **2020**. https://doi.org/10.1155/2020/8881118.

Hagos, M. 2019 Review on: impact of climate change on crop water requirement in Ethiopia. *International Journal of Novel Research in Life Sciences* **6** (5), 24–34.

IPCC 2013 The Physical Science Basis. In: *Contribution of Working Group I to the Fifth Assessment Report of the Intergovernmental Panel on Climate Change* (T. F. Stocker, D. Qin, G.-K. Plattner, M. Tignor, S. K. Allen, J. Boschung, A. Nauels, Y. Xia, V. Bex & P. M. Midgley, eds.). Cambridge University Press, Cambridge, UK, NY, USA.

IPCC 2014 *Summary for Policymakers Integrated View of Climate Change as the Final Part of the IPCC's Fifth Assessment Report (AR5)*.

Jiménez Cisneros, B. E., Oki, T., Arnell, N. W., Benito, G. & Nishijima, A. 2014 *Climate Change Impacts, Adaptation, and Vulnerability in Freshwater resources.: Part A: Global and Sectoral Aspects*. Cambridge University Press, Cambridge, UK.

Joosten, K. & Grey, S. 2017 *Integrating Climate Change Adaptation and Mitigation Into the Watershed Management Approach in Eastern Africa: Discussion Paper and Good Practices Booklet*.

Kuma, H. G., Feyessa, F. F. & Demissie, T. A. 2021 Hydrologic responses to climate and land-use/land-cover changes in the Bilate catchment, Southern Ethiopia. *Journal of Water and Climate Change* **12** (8), 3750–3769. https://doi.org/10.2166/wcc.2021.281.

Legesse, S., Tadele, K. & Mariam, B. G. 2015 Potential impacts of climate change on the hydrology and water resources availability of didessa catchment, Blue Nile River Basin, Ethiopia. **4** (1), 1–7. https://doi.org/10.4172/2329-6755.1000193.

Luo, M., Liu, T., Meng, F., Duan, Y., Frankl, A., Bao, A. & De Maeyer, P. 2018 Comparing bias correction methods used in downscaling precipitation and temperature from regional climate models: a case study from the Kaidu River Basin in Western China. *Water (Switzerland)* **10** (8). https://doi.org/10.3390/w10081046.

Moriasi, D. N., Arnold, J. G., Liew, M. W. V., Bingner, R. L., Harmel, R. D. & Veith, T. L. 2007 Model evaluation guidelines for systematic quantification of accuracy in watershed simulations. *Transactions of American Society of Agricultural and Biological Engineers* **50** (3), 885–900.

Musau, J., Sang, J., Gathenya, J. & Luedeling, E. 2015 Hydrological responses to climate change in Mt. Elgon watersheds. *Journal of Hydrology: Regional Studies* **3**, 233–246.

Neitsch, S. L., Arnold, J. G., Kiniry, J. R., Williams, J. R. & King, K. W. 2002 Soil and water assessment tool theoretical documentation version 2000. *Via MediciTexas Water Resources Institute, College Station, Texas TWRI Report TR-191* **13** (4), 52–55. https://doi.org/10.1055/s-0029-1192096.

Rakhimova, M., Liu, T., Bissenbayeva, S., Mukanov, Y., Gafforov, K. S., Bekpergenova, Z. & Gulakhmadov, A. 2020 Assessment of the impacts of climate change and human activities on runoff in the buqtyrma River Basin, Kazakhstan. *Sustainability (Switzerland)* **12** (12), 4968.

Raneesh, K. Y. 2014 Impact of climate change on water resources. *Journal of Earth Science & Climatic Change* **5** (3). https://doi.org/10.4172/2157-7617.1000185.

Shiferaw, H., Gebremedhin, A., Gebretsadkan, T. & Zenebe, A. 2018 Modelling hydrological response under climate change scenarios using SWAT model: the case of Ilala watershed, Northern Ethiopia. *Modeling Earth Systems and Environment* **4** (1), 437–449. https://doi.org/10.1007/s40808-018-0439-8.

Tesfaye, G. 2017 Land use pattern and its implication on hydrology, climate and degradation in Ethiopia; a review. *International Journal of Agricultural and Environmental Research* **3**, 418–426.

Teutschbein, C. & Seibert, J. 2012 Bias correction of regional climate model simulations for hydrological climate-change impact studies: review and evaluation of different methods. *Journal of Hydrology* **456–457**, 12–29. https://doi.org/10.1016/j.jhydrol.2012.05.052.

Teutschbein, C., Grabs, T., Karlsen, R. H., Laudon, H. & Bishop, K. 2015 Hydrological response to changing climate conditions: spatial streamflow variability in the boreal region. *Water Resources Research* **51** (12), 9425–9446.

Van Vuuren, D. P., Edmonds, J. A., Kainuma, M., Riahi, K. & Weyant, J. 2011 A special issue on the RCPs. *Climatic Change* **109** (1), 1–4. https://doi.org/10.1007/s10584-011-0157-y.

Wagesho, N., Jain, M. K. & Goel, N. K. 2013 Effect of climate change on runoff generation: Application to Rift Valley Lakes Basin of Ethiopia. **18**, 1048–1063. https://doi.org/10.1061/(ASCE)HE.1943-5584.0000647.

World Bank Climate Profile. 2014. Available from: http://sdwebx.worldbank.org/climateportalb/home.cfm?page=country_profile&CCode=ETH&ThisTab=ClimateFuture (accessed 20 June 2014).

Yan, D., Werners, S. E., Ludwig, F. & Huang, H. Q. 2015 Hydrological response to climate change: The Pearl River, China under different RCP scenarios. *Journal of Hydrology: Regional Studies* **4**, 228–245.

Zhang, B., Shrestha, N. K., Daggupati, P., Rudra, R., Shukla, R., Kaur, B. & Hou, J. 2018 Quantifying the impacts of climate change on streamflow dynamics of two major rivers of the Northern Lake Erie basin in Canada. *Sustainability (Switzerland)* **10** (8). https://doi.org/10.3390/su10082897.

First received 9 July 2022; accepted in revised form 27 February 2023. Available online 22 March 2023